Konya Mühendislik Bilimleri Dergisi, c.14, s.3, 1125-1143, 2026
Konya Journal of Engineering Sciences, v.14, n.3, 1125-1143, 2026
ISSN: 2667-8055 (Electronic)
DOI: 10.36306/konjes.1770605

RADIATIVE-SOLAR HEATING TEXTILES WITH ADAPTIVE PERMEABILITY: RECYCLED SILK FIBROIN–GRAPHENE OXIDE COMPOSITE FOR PERSONAL THERMAL MANAGEMENT

[1,*]Nazife KORKMAZ MEMİŞ, [2]Havvanur UYGUR

[1,2] *Süleyman Demirel University, Engineering and Natural Sciences Faculty, Textile Engineering Department, Isparta, Türkiye*
[1]nazifekorkmaz@sdu.edu.tr , [2]havva_uygr@hotmail.com

Highlights

- Passive radiative-solar heating textiles with adaptive permeability were developed.
- SF-rGO composite coated fabrics exhibited radiative heating due to lower mid-infrared emissivity.
- Enhanced photothermal conversion capability of rGO resulted in solar heating.
- Adaptive comfort feature was achieved by humidity sensitive permeability.

Graphical Abstract

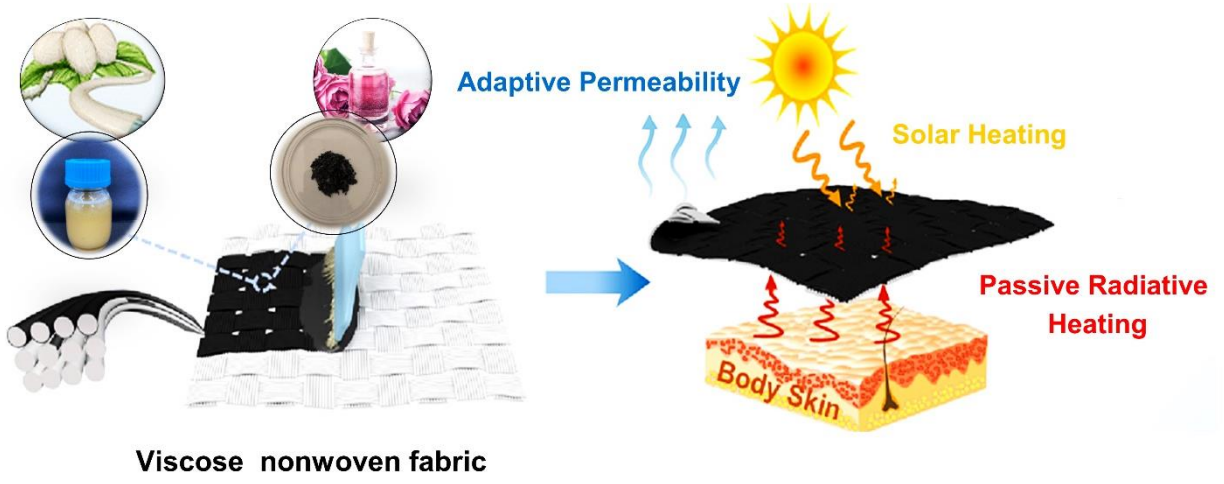


Figure Schematic representation of the composite coated functional fabric for personal thermal management

***Corresponding Author:** Nazife KORKMAZ MEMİŞ, nazifekorkmaz@sdu.edu.tr

Konya Mühendislik Bilimleri Dergisi, c.14, s.3, 1125-1143, 2026
Konya Journal of Engineering Sciences, v.14, n.3, 1125-1143, 2026
ISSN: 2667-8055 (Electronic)
DOI: 10.36306/konjes.1770605

RADIATIVE-SOLAR HEATING TEXTILES WITH ADAPTIVE PERMEABILITY: RECYCLED SILK FIBROIN–GRAPHENE OXIDE COMPOSITE FOR PERSONAL THERMAL MANAGEMENT

[1,*]Nazife KORKMAZ MEMİŞ, [2]Havvanur UYGUR

[1,2]*Süleyman Demirel University, Engineering and Natural Sciences Faculty, Textile Engineering Department, Isparta, Türkiye*
[1]nazifekorkmaz@sdu.edu.tr , [2]havva_uygr@hotmail.com

(Received: 22.08.2025; Accepted in Revised Form: 30.12.2025)

ABSTRACT: Recently, passive heating textiles that manage sunlight and radiation energy without consuming energy have attracted attention as a potential solution for personal thermal management in cold environments. However, static solar energy and/or radiation heating performance may negatively affect comfort and human health. Therefore, there is a need for adaptive textiles that can provide comfort and safety in relation to temperature increase and sweating in cold environments. Herein, passive radiative-solar heating textiles with adaptive permeability were developed by coating viscose nonwoven fabrics (CV-NFs) through composite including fibroin (SF) obtained from upcycled waste silkworm cocoons and rose-water reduced graphene oxide (rGO) particles. Notably, fabrics coated with SF-rGO$_4$ composite containing 4 wt.% particle, exhibited passive radiative heating performance with temperature increase of 2.01°C due to lower mid-infrared emissivity. Also, these samples demonstrated temperature increase of 5.79°C under 0.6 sun irradiation and 10.83°C under real outdoor conditions, respectively thanks to higher solar absorptivity. Besides radiative-solar heating capability and mechanical strength, adaptive comfort feature was been achieved via humidity hence sweat-sensitive permeability by virtue of SF-rGO composite coating. Based on these results, this study offers a sustainable strategy for developing heating textiles with adaptive permeability performance through upcycling of waste silkworm cocoons and eco-friendly reduction method.

Keywords: *Passive radiative heating, Reduced graphene oxide, Rose water, Silk fibroin, Solar heating, Upcycling.*

1. INTRODUCTION

In recent years, the integration of smart technologies into conventional textile materials has enabled these materials to autonomously or on demand heat, cool, and keep the entire body or specific areas dry by adapting to changing environmental conditions. Among these technologies, personal thermal management (PTM) materials which could only cool/heat around human body have overtaken traditional methods thanks to their high-efficiency and energy-saving performance with minimal energy consumption and carbon emissions [1]. Radiative thermal management textiles, one type of PTM, are promising materials for passive heating/cooling without any energy input by controlling natural radiation energy component such as emissivity, transmissivity, reflectivity, and absorption mechanisms [2]. Specifically, heating textiles with natural radiation management capability can control the body's radiation heat transfer path by blocking or suppressing radiation energy [3]-[5]. The heating mechanism of these materials differs for outdoor conditions with sunlight and indoor without sunlight. For indoor radiative heating, textiles should exhibit mid-infrared thermal insulation performance through (i) higher mid-infrared (>2.5 μm) reflectivity of the inner surface to direct body radiation back toward the skin and/or (ii) lower mid-infrared emissivity of the outer surface to suppress body heat dissipation. In addition to this mechanism, textiles should have higher solar absorption hence conversion capability of sunlight into heat energy (photothermal conversion effect) for outdoor conditions with sunlight [6]-[9]. Among these mechanisms, lower mid-infrared emissivity and solar heating are particularly noteworthy in the development of passive radiative heating textiles.

***Corresponding Author:** Nazife KORKMAZ MEMİŞ, nazifekorkmaz@sdu.edu.tr

Lower mid-infrared emittance in the outer layer of a garment can prevent body heat transmission to the external environment, thereby achieving passive radiative body heating. These textile materials have been usually designed by using metal layer coating or metal nanoparticle loading such as silver nanowires [10], copper [11], gold [12], and/or alloy materials, etc. Indoor passive heating performance has been achieved with through the aforementioned and materials without any energy input however they are expensive, less practical, and not easily wearable, making it difficult to be widely used. Therefore, nowadays researchers are focused on developing heating textile materials that could fully be employed in daily life under both indoor and outdoor conditions. Besides lower mid-infrared emissivity, solar radiation is a renewable and eco-friendly energy for heating materials through thermal energy conversion performance with photothermal effect. Textiles could have solar heating performance by using high solar absorption hence photothermal conversion materials. In recent years, various methods have been proposed to increase the solar absorption of materials such as graphene [13], metallic reflectors [14], [15], plasmonic nanostructures [16], [17], and two-dimensional materials with photonic crystal nanocavities [18]-[21], biomimetic photothermal materials [22], [23] to effectively utilize solar energy. Also, metals [24], metal oxides [25], metal carbides such as zirconium carbide, MXene [26], [27], metal sulfides [28], and conjugated polymer materials [29], [30], have been used in developing heating textile structures using the photothermal conversion mechanism, either as a fabric coating or an embedded fiber. Although various materials and methods outlined above are employed in developing heating textile structures through the photothermal conversion mechanism, there is still a notable gap in research focused on enhancing the solar absorbance of textiles [31]. In this context, enhancing solar absorption hence photothermal conversion capacity and integration lower emissivity could be an energy-saving approach for all-day comfort in cold environments. In this regard, rGO particles obtained by reducing graphene oxide particles in recent years can provide passive heating effect by increasing the heating rate of the material [32] and reducing mid-infrared emissivity.

Reducing agents such as hydrazine/hydrazine derivatives or sodium borohydride, commonly used to reduce graphene oxide particles are effective but toxic. Therefore, in recent years, antioxidants obtained from ascorbic acid, sugar, bovine serum albumin, heparin, and plant extracts have attracted attention as environmentally friendly and inexpensive reducing agents [33], [34]. It is well known that commercial Rosa damascene (rose water) may demonstrate its potential for use as a cheap and environmentally friendly material in developing reduced graphene oxide particles from graphene oxide particles thanks to phenolic and flavonoid compounds [33], [35].

Even though efficient passive heating could be achieved by integrating of enhanced solar absorptivity and lower mid-infrared emissivity, static solar energy and/or radiation heating performance which can lead to heating levels that may negatively affect comfort and human health [36], is a dilemma. Accordingly, there is a need for a dynamic thermal management system that can provide comfort and safety in relation to temperature increase and sweating [37]. Water/moisture hence sweat-sensitive materials could change the micro and macro structure of textile materials and thus provide comfort through dynamic performance especially permeability [38]. In recent years, alongside growing concerns about the environmental impact and costs of fossil fuels, there has been a notable increase in demand for products derived from renewable and sustainable sources. In this context, researchers have focused on hydrophilic particles and biopolymers that can form reversible bonds with water molecules, enabling water/moisture-adaptive permeability performance in textile material using nano-scale particles derived from renewable sources [36]. Among these biopolymers, silk fibroin is a protein substance containing tyrosine and serine with a high percentage of -OH groups in its structure, contact with sweat and/or water enables the -H bonds between the α-helix and β-sheet molecular structure to form reversible bonds with water molecules [39]. Fibroin can be extracted from currently high amounts of dissolved cocoons, silkworm farming waste, cocoon dissolution, silk spinning, and silk weaving waste. Although individual strategies for passive heating and adaptive permeability already exist, a comprehensive approach integrating sustainable upcycling of waste materials (silk fibroin), eco-friendly green synthesis (rose water-reduced graphene oxide) with and the simultaneous achievement of dual-mode radiative-solar

heating with humidity/sweat-sensitive permeability, has not yet been reported. Such a multifunctional and environmentally conscious design represents a significant advancement toward practical and sustainable personal thermal management.

To address this gap, this study proposes a novel composite coating onto CV-NFs, utilizing the unique properties of upcycled SF and rGO particles as nanofillers for adaptive permeability and radiative-solar heating performance, respectively. Fibroin particles, one of nanofillers, were obtained through the upcycling of waste silk cocoons. The other nanofiller, rGO particles, was reduced by using commercial Rosa damascene (rose water) which a local and environmentally friendly material for enhanced radiative-solar heating function. These active components are integrated within a transparent, flexible and durable thermoplastic polyurethane (TPU) matrix to develop a versatile textile capable of adaptive personal thermal management. In addition to morphological and chemical characterization, the optical characteristic of the samples was systematically determined by using transmission and reflection data obtained from FT-IR and UV-VIS spectrophotometers with reflecting spheres. Also, radiative-solar heating performance tests were conducted under simulated conditions by a self-designed hotplate system and real-life measurements in both sweating and dry conditions. This study offers an alternative strategy for a smart textile material capable of dual radiative-solar heating under both indoor and outdoor conditions, with adaptive permeability and waste utilization effect.

2. MATERIALS AND METHODS

2.1. Materials

In this study, CV-NFs (65 g/m^2, 0.6 mm) were used as the substrate for composite-coated textile materials with adaptive moisture permeability and radiative-solar heating performance. For developing composite coating material, TPU pellets (Elastollan 1185A) obtained from BASF Polyurethanes GmbH, were used as matrix material due to their high transparency, elasticity, tensile strength, wear resistance, and corrosion resistance [40]. These TPU pellets were dried at 60°C for 24 h in an oven prior to usage. N, N-Dimethylformamide (DMF) (Merck, Germany) and acetone (ACE) (Merck, Germany) were as solvent and co-solvent, respectively to dissolve TPU pellets. Waste silkworm cocoons were provided by Umurbey Silk Production and Design Center in Bursa, Türkiye to get SF particles for adaptive moisture permeability. Sodium carbonate (Na_2CO_3) (ZAG Chemical, Türkiye), anhydrous calcium chloride ($CaCl_2$) (Merck, Germany), and ethanol (EtOH) (Merck, Germany) were used in SF extraction process. Graphene oxide particles (GO, 2-5 layer, size: 5-40 μm, surface area: 420 m^2/gr) were purchased from Nanografi, Türkiye to obtain rGO particles for radiative-solar heating performance. Commercial Rosa damascene (rose water) as a green reducing agent was purchased from Gülbirlik-Rosense®, Türkiye.

2.2. Preparation of SF and rGO Particles

A simultaneous passive radiative-solar heating and adaptive permeable textiles through composite coating onto CV-NFs as shown schematically in Figure 1, which involves preparation of SF and rGO particles and TPU-SF@rGO composite coating. As seen in Figure 1 (a), waste silk cocoons were first cut into small pieces and cleaned of silkworm residues for SF extraction. Subsequently, the cleaned silkworm cocoon shells were boiled in a 0.5 wt.% Na_2CO_3 solution at 95°C for 1 h (liquor ratio: 70:1) to remove the sericin. The silk fibres were then separated by washing three times in deionised water at 60°C and drying at 50°C for 3 h. These degummed silk fibers (14 g) were dissolved in the solution of $CaCl_2$: EtOH: H_2O (280 ml) in molar rate of 1:2:8 at 60°C for 6 h. After 24 h of dialysis using a 10.000 MWCO tubing (Sigma Aldrich, USA), the SF solution was centrifuged at 10.000 rpm for 15 min (HettichRotina 380 R) to remove impurities and achieve a homogeneous solution. This SF solution was initially freeze-dried at -80°C and then lyophilised at -55°C for 72 h using a Labconco Centrivap Micro IR to get powder. The powder was milled into particles with <40 μm diameter using a micro powder pulveriser (Fritsch Pulverisette, Germany) and then sieved through a 40 μm sieve. These SF microparticles were stored at 4°C until use.

Thanks to phenolic and flavonoid compounds [35], commercial Rosa damascene (rose water) obtained in Isparta was preferred as green reduction agent to synthesize rGO. In green reduction process as shown in Figure 1 (b), initially GO particles were dispersed in deionized water (3 mM) through mechanically stirring for 3 h and subsequently bath sonication for 30 min. Subsequently, the prepared GO suspension was mixed into 12% commercial rose water with a 1:1 volume ratio at 100°C for 6 h. Finally, this solution was centrifuged at 10.000 rpm for 15 min, washed repeatedly with deionized water for eliminating of any reducing agent, and dried at 60°C for 24 h in an oven [33], [34]. The resulted black rGO powder was characterized by FT-IR.

2.3. Preparation of TPU-SF@rGO Composite Coated CV-NFs

A simple spraying and drying process was used for preparation of TPU-SF@rGO composite-coated CV fabrics, as shown in Figure 1 (c). In the coating process, initially TPU solution at 10 wt.% was prepared through dissolving TPU pellets in DMF:ACE mixing with a volume ratio of 1:1 using a mechanical stirrer at 60°C, 400 rpm for 6 h. After that, SF particles at 2 wt.% were added into TPU solution and mixed using mechanical stirring for another 3 h followed rGO particle adding at 1-4 wt.%. The obtained TPU-SF@rGO composite dispersions were mixed mechanically for 3 h and additional 30 min bath sonication. In the next step, TPU-SF@rGO composite dispersions were deposited on the surface of CV-NFs by using an Alfajet W-77S (Türkiye) manual spraying system. Finally, coated samples were dried room temperature for 24 h. Also, TPU and TPU-SF composite-coated samples were prepared through the same procedure to determine the effect of rGO particles on radiative-solar heating performance. The TPU, TPU-SF, TPU-SF@rGO$_x$ (x denoted rGO content), and TPU-SF@GO$_x$ coated CV-NFs were named as CV_T, CV_TF, CV_TFR$_x$, and CV_TFG$_x$, respectively. The reference sample without any coating was coded as CV.

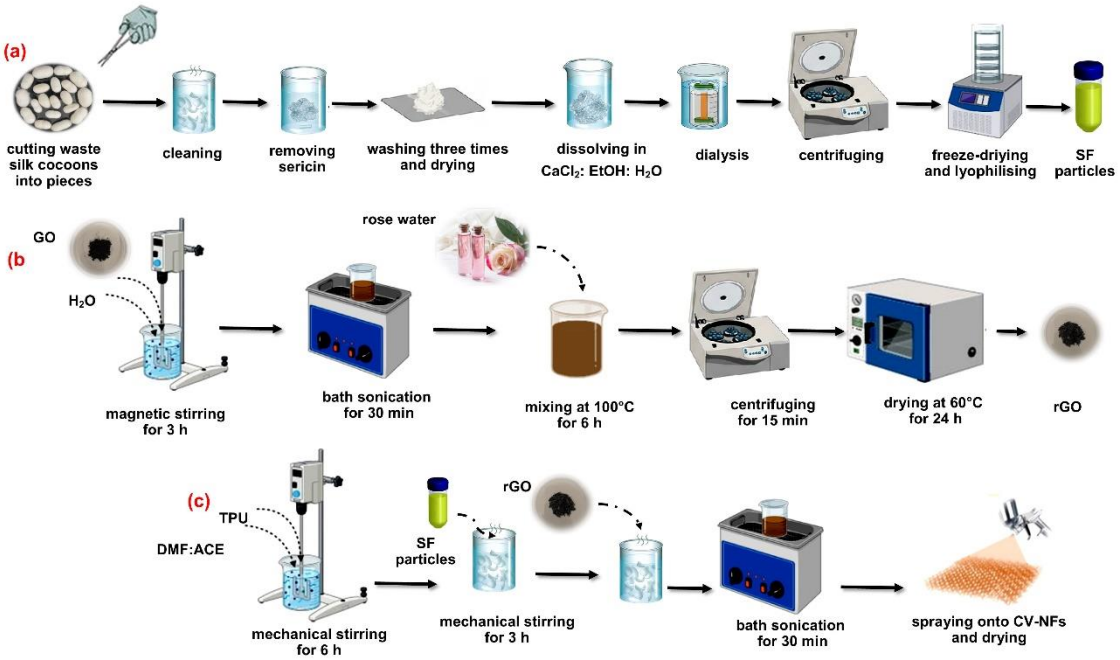


Figure 1. Flow chart of the SF (a) and rGO (b) particles, and composite coating onto CV-NFs (c)

2.4. Characterizations

2.4.1. Materials characterizations

Microstructure and surface morphology of the reference and coated CV-NF samples were characterized using Scanning electron microscopy (SEM) (Fei Quanta FEG 250) at an acceleration voltage of 20 kV, 10 μA current, and 500-1000 magnification. Chemical composition of the samples was analysed by Fourier transform infrared (FT-IR) spectrometer (JASCO FT/IR 4700) equipped with a diamond ATR

(Attenuated total reflectance) in the 400-4000 cm^{-1} range, 2 cm^{-1} resolution, and 16 scan at room temperature. An UV-Vis-NIR spectrometer (JASCO V-770 UV-Vis-NIR) integrated with a diffuse integrating sphere was used for recording solar reflectance and transmissivity of the samples in the wavelength range of 0.19-2.7 μm. Also, a FT-IR spectrometer (Bruker VERTEX 70v) coupled with an MIR integrating sphere in the diffuse reflectance mode was used to record the reflectance ($\rho(\lambda)$) and transmittance ($\tau(\lambda)$) of the samples in the atmospheric window wavelength ranges (8-14 μm). According to Kirchhoff's Law, the spectral absorptivity ($\alpha(\lambda)$) = emissivity ($\varepsilon(\lambda)$) when an object in thermodynamic equilibrium; thus, $\alpha(\lambda)$ or $\varepsilon(\lambda)$ can be calculated as $\varepsilon(\lambda)/\alpha(\lambda) = 1 - \rho(\lambda) - \tau(\lambda)$. The average value solar absorptivity and atmospheric window emissivity were calculated according to Equation (1) and Equation (2), respectively.

$$\bar{\alpha}_{solar} = \frac{\int_{0.3\ \mu m}^{2.5\ \mu m} I_{solar}(\lambda)\alpha(\lambda)d\lambda}{\int_{0.3\ \mu m}^{2.5 \mu m} I_{solar}(\lambda)d\lambda} \quad (1)$$

$$\bar{\varepsilon}_{IR} = \frac{\int_{8\ \mu m}^{14\ \mu m} I_{BB}(\lambda)\varepsilon(\lambda)d\lambda}{\int_{8\ \mu m}^{14\ \mu m} I_{BB}(\lambda)d\lambda} \quad (2)$$

where ε: emissivity, α: absorptivity, ρ: reflectance, τ: transmittance, and λ: wavelength, $I_{solar}(\lambda)$: global solar intensity spectrum according to ASTM G173, I_{BB}: spectral radiance of a blackbody defined by Planck's law at temperature T.

2.4.2. Radiative and solar heating performance measurement

Simulated heating performance measurement

Indoor radiative heating performance of the samples based on low-emissivity without any solar heating effect, was measured using a designed hotplate system simulating skin shown in Figure 2. This self-made system consists of heating sheet, 8 K-type sensors, and a data acquisition system. The heating sheet was employed to simulate the metabolic heat generation (34°C) and acted as the human skin. The actual temperature of the samples was measured at every 10 s for 1 min while stabilizing and 30 min with environment temperature at 21-24°C and relative humidity at 56-59%.

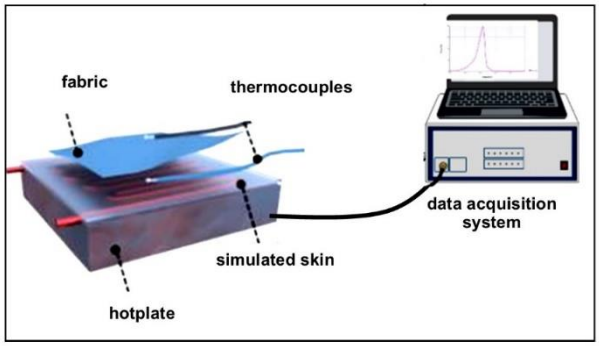


Figure 2. Schematic illustration of the designed hotplate system simulating skin for indoor measurement

As for the solar heating performance, a sun simulator halogen lamp was integrated into the designed hotplate system, shown in Figure 3, for indoor photo-thermal conversion simulation test. The samples placed on the hot plate under lamp's switched-on period with 600 W/m^2 simulated solar light intensity and switched-off period for 30 min, respectively via recording one data per ten second. For both radiative and solar heating performance measurement, the average temperature on the sample's lower surface was determined by performing least three replications.

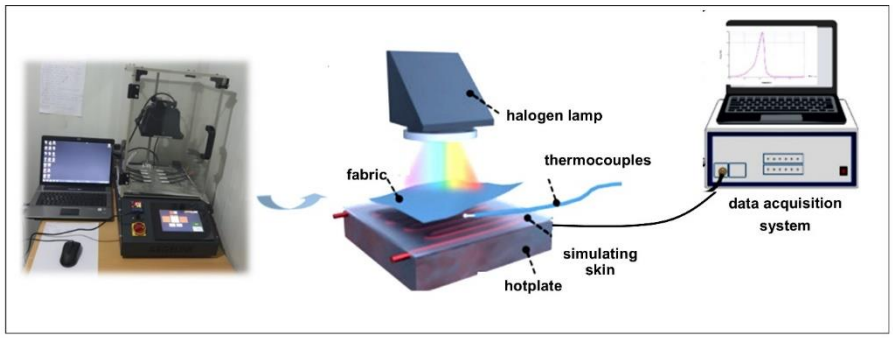


Figure 3. Digital photo and schematic diagram of the designed hotplate system simulating skin with a sun simulator halogen lamp

Also, the effect of water/humidity hence sweat in indoor conditions, 0.1 ml of deionized water was dropped on each sample for each sample and then tests were carried out using these wet samples with the same procedures.

A comprehensive heating performance calculation method was described below:

T_0 : Initial temperatures of the samples measured by sensors for 1 min.

T_{max}: The maximum temperature measured after 30 min of the lamp-on stage.

T_{end}: The minimum temperature measured after 30 min of the lamp-off stage.

Heating performance was calculated comparatively as $\Delta T_{max}=T_{maxcoated}-T_{maxCV}$

Heat storage performance was calculated as $\Delta T_{heating} = T_{max} - T_0$

Heat retention performance were calculated as $\Delta T_{cooling} = T_{max} - T_{end}$

Outdoor real-time heating measurement

Outdoor real-time heating measurements of the samples were conducted at Süleyman Demirel University, Textile Engineering Laboratory, West Campus (Isparta, Türkiye, 37° 49' 42'' N, 30° 31' 34''E). A self-designed test setup including polystyrene foam box in size of 20×20×12 cm^3 and coated with aluminium foil for minimizing heat transfer. The top opening of the hollowed-out insulating foam box was covered with properly sized samples, and K-type thermocouples were fixed to the bottom of the samples for recording temperature variation in real-time. To avoid errors arising from thermal effects on the test temperature, this self-designed test setup was placed on a bench 1 m above the ground. The temperature of the samples was recorded every 5 s using a multichannel type K thermocouple (TET-640) recorder (KIMO KTH 320).

As for the water/humidity hence sweat-adaptive outdoor heating measurement, 10×3 cm^2 cylindrical grooves were opened at the top of 20×20×12 cm^3 polystyrene foam box in the self-designed test setup (Figure 4). After placing water-filled sponges in each groove with the tested sample covered on the surface, the outdoor heating performance was evaluated by recording the temperature below the samples using multichannel datalogger.

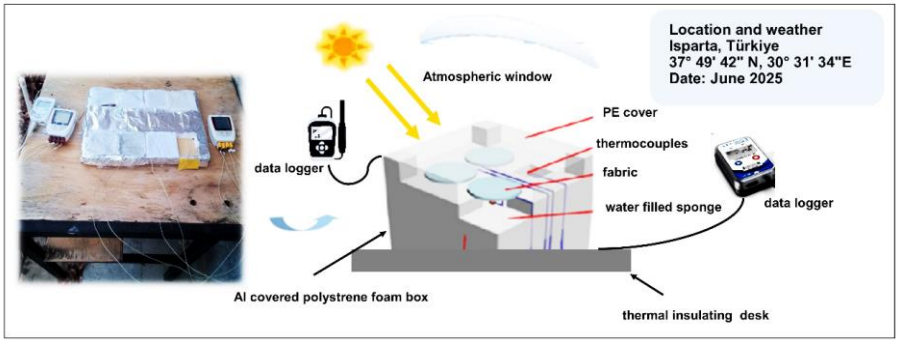


Figure 4. Digital photo and schematic diagram of the self-designed test setup for sweat-adaptive outdoor heating measurement

2.4.3. Wearable performance evaluations

To evaluate wearability performance of the developed samples, physical, mechanical, and permeability tests were conducted. Physical (weight) and mechanical (bending rigidity, tensile stress-strain properties) properties were determined according to ASTM D3776/D3776M-20, ASTM D1388 (2002), and ASTM D5035-95 (2003) standards, respectively for determining coating effect. A universal material tensile tester (Llyod Instruments LR5K+) was used to measure tensile stress-strain properties in uniaxial tests mode with 75 mm test length and 300 mm/min speed, in turn. Air permeability was measured using a FX 3300 Textest (James Heal Corp., UK) automatic fabric permeability meter according to TS 391 EN ISO 9237 standard under 200 Pa pressure with at least ten replicates. Also, adaptive moisture permeability performance was dynamically measured followed by ASTM E96-80 standard with modification at different relative humidity values in the range of 40-65% and temperature of 20°C. Briefly, plastic dishes with 41 mm depth and 46 mm diameter were filled with water, creating an air layer with a thickness of 1 cm between water and lower surface of the sample. After sealing samples onto the dishes with epoxy-phenolic adhesive, weight change within 24 h on every 1 h was carefully measured and recorded. Water vapor permeability (WVP) was calculated using Equation (3).

$$WVP = \frac{24\mathrm{M}}{\mathrm{At}} \tag{3}$$

where *WVP* is water vapor permeability (g/m^2/24 h), *M(g)* is the rate of weight change over the time period (24 h), *A* is the test area (m^2), *t* (h) is the time period.

Water absorption ratio (%) was measured according to EDANA 10.3.99 standard. After cutting into proper dimensions and also recording weights of the samples, they were immersed in an aqueous 0.9 wt% NaCl solution using a grid system and held 2 cm below the liquid surface for 1 min. Subsequently, the samples were removed from the water using tweezers and held vertically for 2 min to allow free water to drain away. The maximum absorption capacity (%) was then determined from the difference between the wet and dry weights of the weighed sample.

All test results were statistically evaluated by SPSS 26 for Windows statistical software (IBM, Armonk, USA) using Tukey post hoc test. *p* value less than 0.05 was deemed to be significant for all test results.

3. RESULTS AND DISCUSSION

3.1. Morphology and Microstructure Characterization

In this study, the feasibility of developing radiative–solar heating textiles via eco-friendly processing was investigated, aiming to achieve zero-energy thermal management, dynamic permeability, and waste upcycling. Microstructure and also surface morphology of the reference and coated CV-NFs were observed by SEM as shown in Figure 5. The uncoated CV (Figure 5 (a_1-a_2)) displayed a smooth, porous, and open network structure of CV (reference CV-NFs) with fiber entanglement. All coating treatment resulted in rougher surface structure. As TPU solution spraying created very thin and more blurred coating (Figure 5 (b_1-b_2)), TPU-SF composite adhered fabric surface and among fiber/yarns (Figure 5 (c_1-c_2)). Also, there are many bright spots on the surface of the CV_TF ones (sample coated with TPU-SF) owing to SF particles. SF particles and particle agglomeration resulted in rougher surface can be seen in surface of CV_TF ones (Figure 5 (c_1-c_2)). With the addition of rGO particles to the composite coating, a relatively more homogeneous particle distribution was achieved on the fabric surface (Figure 5 (d_1-e_1)). As the amount of rGO particle increased, the coating amount and particle distribution on the fabric surface enhanced which is an advantage for the radiative-solar heating performance.

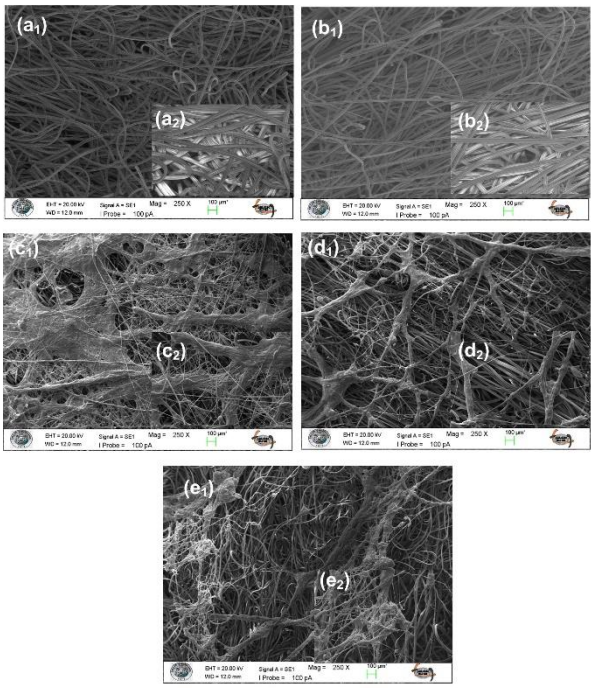


Figure 5. SEM images of the CV (a_1)-(a_2), CV_T (b_1)-(b_2), CV_TF (c_1)-(c_2), CV_TFR$_1$ (d_1)-(d_2), CV_TFR$_4$ (e_1)-(e_2) at 250x and 1000x magnification

To characterize structure of the green synthesized rGO particles and also chemical composition of the samples, the surface functional groups were analysed by FT-IR spectroscopy. As shown in Figure 6, the FT-IR spectrum of GO exhibits characteristic peaks [33], including a strong C=O stretching peak of carboxylic acid and carbonyl groups at 1716 cm^{-1}, broadband in 3686-2900 cm^{-1} attributed to O-H stretching mode of absorbed water, a weak C-OH stretching (carboxyl) peak originating from the carboxylic acid at 1357 cm^{-1}, C-O stretching (epoxy or alkoxy) peak at 1049 cm^{-1}, and a strong C=C stretching peak at 1621 cm^{-1}. Decreasing absorption bands of the oxide groups as seen in the spectrum of rGO particles, is a proof of a successful chemical reduction process using rose water. Moreover, colour change of the particles from brown to black by reduction process supported the green reduction of GO particles.

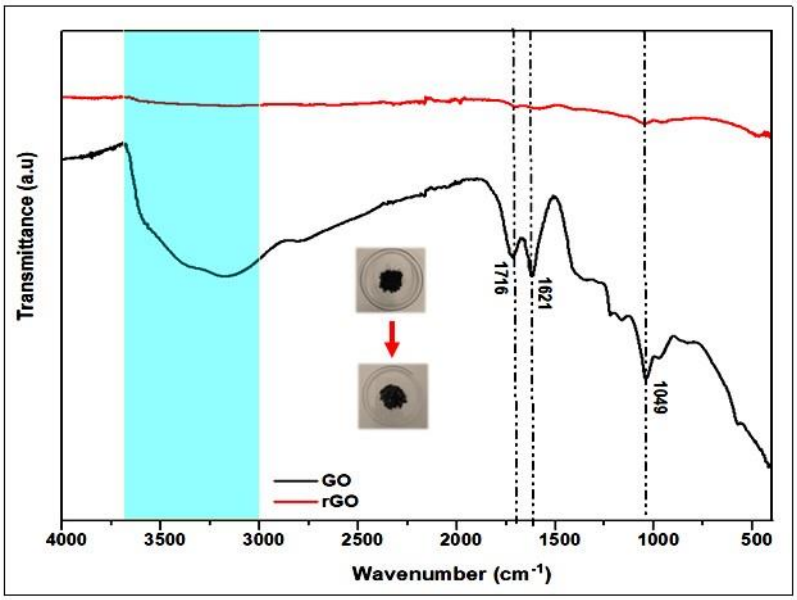


Figure 6. FTIR spectra of GO and green synthesized rGO particles with rose water

FT-IR spectra of the reference CV-NFs (CV) and coated samples were given in Figure 7. The CV samples exhibited the characteristic peaks of polypeptide in the range of 800-1200 cm^{-1}, OH of alcoholic and carboxylic and -C = O bands at 3200-3500 and 1655 cm^{-1}, respectively. Also, the stretching vibrations of the N-H bond, alkene-CH stretching vibrations, and C-O-C stretching vibrations were detected at 3578-3348 cm^{-1}, 2922 and 2855 cm^{-1}, and 1074 cm^{-1} which are characteristic peak of TPU. Besides these functional groups, TPU had free C=O and H-bonded C-O peaks at 1731 and 1701 cm^{-1}. The characteristic peaks of SF particle such as amide I, amide II, and amide III were observed at 1651-1593, 1535, and 1233 cm^{-1}, arising from C-N stretching, C-N and N-H deformation, respectively [41], [42]. The coated samples displayed all of these characteristic peaks in their IR spectra. Since rGO particles do not have distinct infrared characteristic peaks, rGO including samples (CV_TFR_1 and CV_TFR_4) and CV_TF had similar IR spectra.

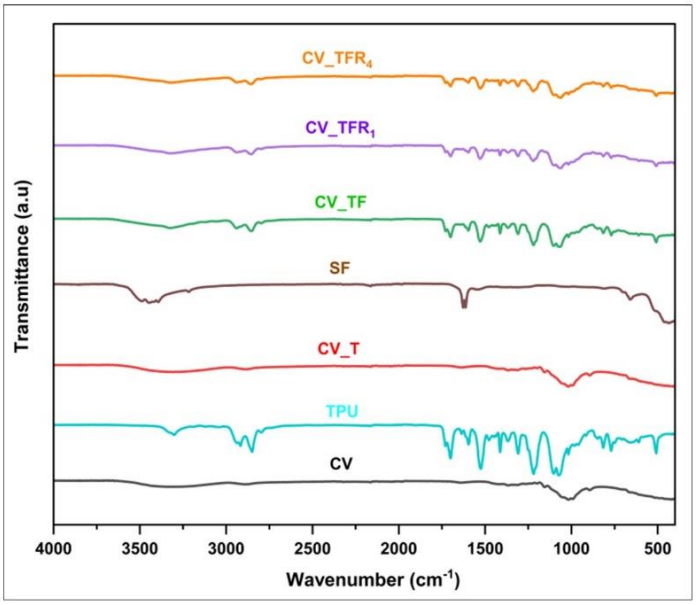


Figure 7. FT-IR spectra of TPU polymer, SF particle, and the fabrics

3.2. Simulated Heating Performance

3.2.1. Radiative passive heating performance

Reducing mid-infrared emissivity of the fabric surface hence thermal radiation loss of human body is a necessary parameter to generate passive radiative heating performance for indoor thermal management without any solar effect. The mid-infrared reflectance and transmittance of samples were measured by FT-IR spectrometer equipped with an MIR integrating sphere. Emissivity (ε) based on thermal radiation and also $\bar{\varepsilon}_{IR}$ are calculated in the atmospheric window wavelength ranges (8-14 μm). As shown in Figure 8 (a), while TPU and TPU-SF composite coating enhanced mid-infrared emissivity of the CV, CV_TFR_1 and especially CV_TFR_4 exhibited low thermal emissivity within the mid-infrared spectrum, limiting the dissipation of human body heat to achieve indoor warming [8], [9]. The CV ones had an $\bar{\varepsilon}_{IR}$ of 81.92%, which increased with TPU coating and reached up to maximum value of 85.66% for the CV_TF ones. Conversely, rGO particle addition resulted in decrease of $\bar{\varepsilon}_{IR}$ to 80.97 and 75.44%, respectively. The minimum $\bar{\varepsilon}_{IR}$ value hence higher passive radiative heating ability belonged to CV_TFR_4 ones. Furthermore, the passive radiative heating ability of the samples was evaluated and compared through temperature change recording with a designed hotplate system simulating skin for 30 min. Real time temperature curve and also lower surface' maximum temperature of the samples are given in Figure 8 (b) and Figure 8 (c), respectively. CV_TFR_4 exhibited the maximum temperature (34.05°C), followed by CV_TFR_1 and CV_TF (33.67°C) and bare skin had the minimum temperature (31.99°C), as seen in Figure 8. The maximum temperature of CV_TFR_4 was 2.01°C and 2.06°C higher than that of the CV and bare skin, in turn. According to literature [10], [43] the 2.06°C radiative heating temperature can provide energy saving of approximately 10% of building heating energy consumption, which is a potential approach for

tackling global climate change. These results indicate that coated fabrics especially CV_TFR4 can heat human body based on low mid-infrared emissivity without any energy input.

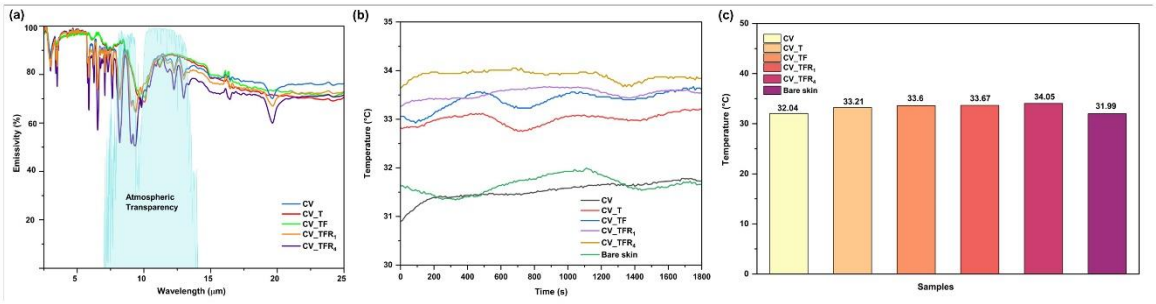


Figure 8. Infrared emissivity spectra (a), real time temperature curve (b), and lower surface' maximum temperature values without sun simulator (c) of the fabrics

3.2.2. Solar heating performance

Solar energy as a clean and renewable energy, has attracted attention thanks to large thermal energy conversion capacity. Thermal energy conversion performance with photothermal effect (solar radiation (sunlight) conversion into thermal) varies solar the absorption capacity of materials [8]. For outdoor heating performance including solar effect, as well as low mid-infrared emissivity, higher solar absorption ability is crucial. To evaluate solar absorption hence heating performance of the samples, solar reflectance and transmittance were measured by UV-Vis-NIR spectrometer equipped with an integrating sphere and solar absorptivity (α) and average value ($\bar{\alpha}_{solar}$) were calculated in corresponding wavelength (0.3-2.5 μm). As shown in Figure 9, coated samples especially CV_TFR4 ones had higher solar absorptivity. As the CV samples had $\bar{\alpha}_{solar}$of 43.99%, this value also photothermal conversion performance increased and reached up to maximum value of 69.43% in CV_TFR4 ones followed by CV_TFR1 with value of 55.48%. $\bar{\alpha}_{solar}$ of the samples significantly varied with rGO amount due to the localized surface plasmon resonance effect and higher solar absorption coefficient [43]. Furthermore, the rougher surface of the CV_TFR samples (seen in SEM images) improved light capture hence photothermal performance as a result of light reflection minimizing and light refraction and internal reflection enhancement [44]. These results indicate that rGO particles enhanced solar absorption hence heating performance.

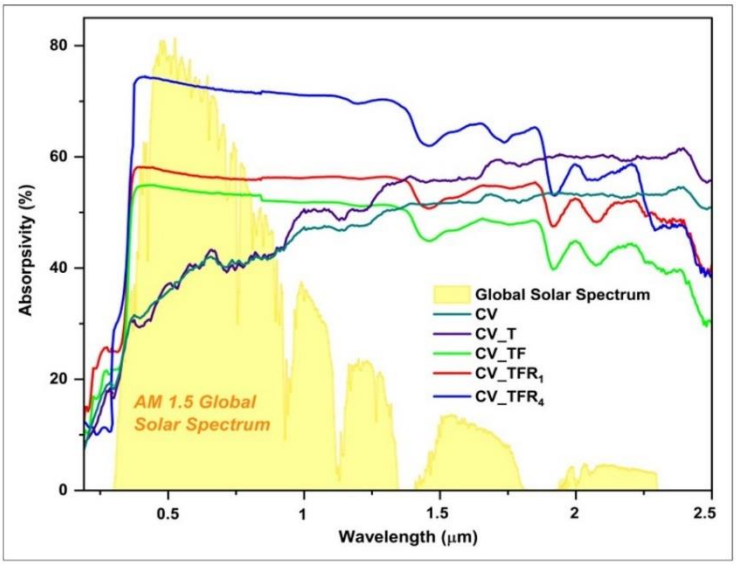


Figure 9. Solar absorptivity spectra of fabrics

The solar heating ability of samples was evaluated and compared through temperature change recording with a designed hotplate system and halogen lamp (600 W/m^2) (0.6 sun) simulating sunlight exposure. The real time temperature curves and also temperature variation of the samples between each other are given in Figure 10 and Table 1, respectively. As seen in Figure 10 and Table 1, the temperature of all samples gradually increased and reached maximum for each sample after 30 min of sunlight exposure. Under 600 W/m^2 solar intensity, CV_T and CV_TF samples finally displayed temperature of 49.94°C and 48.70°C, respectively which is lower than the temperature of the CV ones (50.48°C). On the contrary, the temperature of CV_TFR$_1$ and CV_TFR$_4$ samples reached 54.08°C and 56.27°C after 0.6 standard sunlight irradiation for 30 min. Solar heating effect was detected for composite coating including rGO particle with a temperature increase (ΔT_{max}) of 3.6°C and 5.79°C (Table 1), respectively as compared to the CV ones. Also, the temperature of samples coated with composite coating including GO particle (CV_TFG$_4$) was measured to evaluate the effect of reducing process. As seen in Table 1, this sample had a temperature of 50.51°C, which is nearly similar with the CV ones. These results show that CV-TSF samples especially including 4 wt.% of rGO particles has solar heating performance with higher solar absorption and photothermal conservation ability that could provide thermal comfort in cold conditions without any energy input.

Additionally, heat storage and retention performances during heating ($\Delta T_{heating}$) and cooling ($\Delta T_{cooling}$) with and without sunlight exposure were calculated. For an ideal passive heating material, the maximum temperature increase under the lamp simulating solar ($\Delta T_{heating}$) is targeted for heat storage, while the temperature decrease ($\Delta T_{cooling}$) after switch-off of the lamp should be minimum for heat retention. As temperature increasing values during heating of sunlight exposure were compared (Table 1), the maximum $\Delta T_{heating}$ value was observed for CV_TFR$_4$ samples (22.59), which is an indicator of heat storage performance. On the other hand, after switching off lamp, these samples exhibited lower heat retention performance ($\Delta T_{cooling}$) with higher temperature decreasing (24.24).

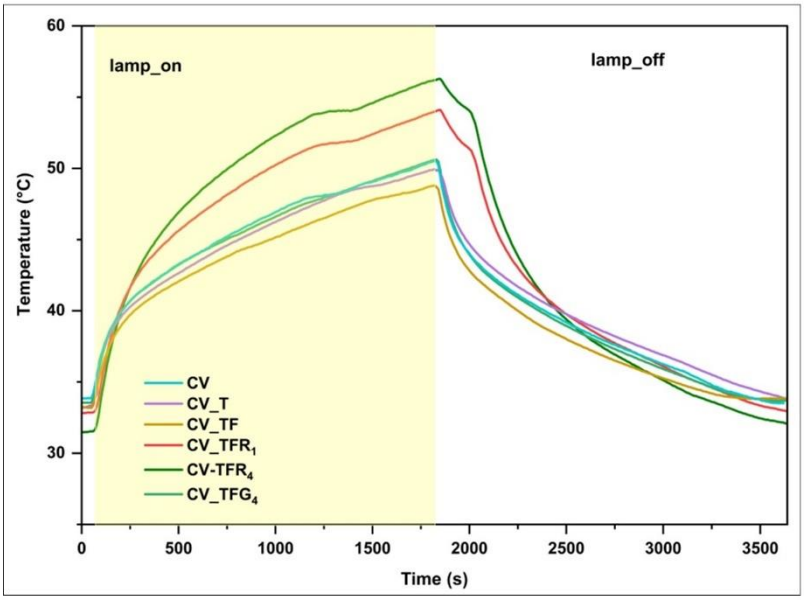


Figure 10. Real time temperature curves of the fabrics with sun simulator

Table 1. Comparative heating performances of the fabrics

Samples	CV	CV_T	CV_TF	CV_TFR$_1$	CV_TFR$_4$	CV_TFG$_4$
T_0	34.42	33.35	33.35	32.87	33.68	33.51
T_{max}	50.48	49.94	48.70	54.08	56.27	50.51
$\Delta T_{heating}$	16.06	16.59	15.35	21.21	22.59	17
T_{end}	33.51	33.85	33.85	32.47	32.03	33.85
$\Delta T_{cooling}$	16.97	16.09	14.85	21.61	24.24	16.66

Effect of humidity/water hence sweating was investigated by an indoor sweat experiment through dropping a certain amount of water on the samples and results are given in Figure 11. As seen in Figure 11, the temperature of CV_TFR and CV significantly decreased due to evaporative cooling, whereas the temperature of CV_T and CV_TF ones keep almost unchanged during sunlight exposure. After sunlight exposure for 30 min, a similar trend was detected with dry samples (Figure 11), the maximum temperature (56.73°C) and also solar heating performance in CV_TFR$_4$ samples. Although, temperature increase of 1.96°C comparing to the CV in wet state is lower than dry state (5.79°C), CV_TFR$_4$ ones still had solar heating performance.

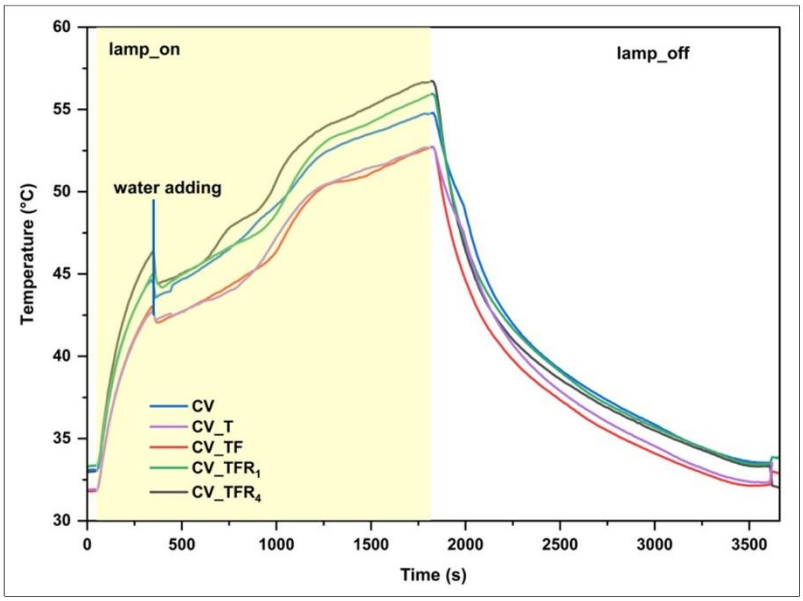


Figure 11. Real time temperature curves of the fabrics with sun simulator under wet conditions

3.3. Outdoor Heating Performance

An outdoor heating experiment was conducted on 20 June 2025 (from 12:55 to 16:33 p.m) at Süleyman Demirel University, Textile Engineering Laboratory, West Campus (Isparta, Türkiye, 37° 49' 42" N, 30° 31' 34" E) to evaluate the actual heating capability of the samples. Outdoor real-time heating measurements of the samples under dry conditions without any water/sweat effect, were given in Figure 12. As seen in Figure 12, CV_TFR$_4$ samples reached maximum temperature of 56.73°C followed by CV_TFR$_1$ ones with temperature of 53.9°C while CV_TF and CV_T ones had maximum temperature of 46.8°C and 47.7°C, respectively. To compare the heating capability, measurements were also taken for a conventional cotton fabric (widely used as clothing) and bare skin. It was observed that the maximum temperature of the cotton fabric and bare skin reached 48.6°C and 45.8°C, which are lower than the CV (45.9°) and CV_TFR ones. CV_TFR samples especially CV_TFR$_4$ ones had approximately 10.83°C, 8.13°C, and 10.93°C higher temperature compared to the CV, cotton, and bare skin, respectively, indicating rGO particles especially

at higher amount providing solar heating performance. Also, these outdoor test results are consistent with indoor simulated test results.

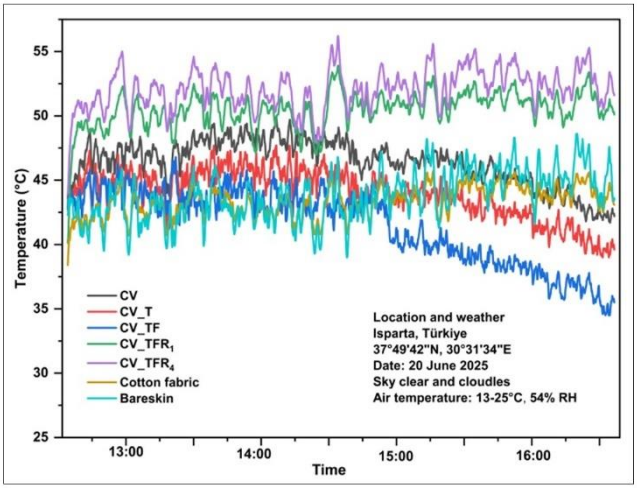


Figure 12. Outdoor real-time heating performance of the fabrics

In addition, water/humidity hence sweat adaptive outdoor heating measurement results were given in Figure 13. As shown in Figure 13, even after adding wet sponge under the samples simulating sweating, the same samples (CV_TFR_4) reached maximum temperature of 46.8°C followed by CV_TFR_1 ones with temperature of 44°C, which are lower than dry conditions. CV_TFR samples especially $CV\text{-}TSR_4$ ones still had solar heating performance despite dissipate excessive heat to the external environment by water evaporation [46]. Overall, CV_TFR_4 samples could warm human body thanks to solar absorption capacity and photothermal conversion efficiency imparted by the rGO particles in both sweating and dry conditions.

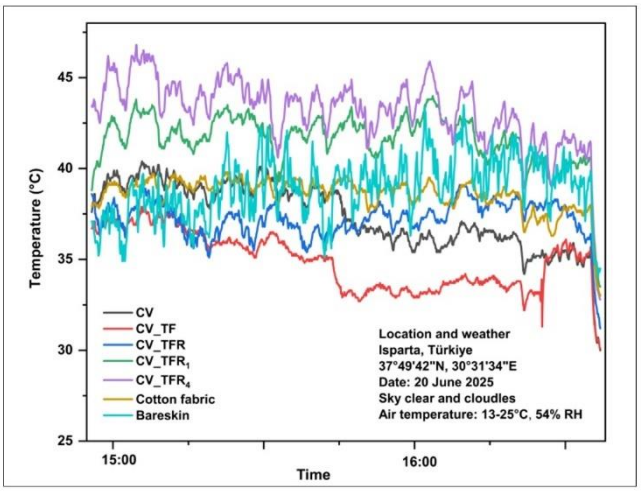


Figure 13. Outdoor real-time heating performance of the fabrics under wet conditions

3.4. Wearability Performance

As well as effective thermal management, wearability performance, one of fundamental requirements for practical applications, must be taken into consideration in the design of functional textiles. To evaluate wearability performance of the samples in practical applications; physical, mechanical, and permeability properties were thoroughly characterized. As detailed in Table 2, all coating types resulted in a notable ($p<0.05$) weight increasing and the maximum values belonged to the coated samples with CV_TFR_4, as expected. Also, rGO particle content significantly affect the sample weight. In addition to weight, bending rigidity values of the samples exhibit increasing with coating especially including SF and rGO particles

(from 42.72 to 210.03 mg.cm) as a result of fiber inter-fibre spaces' coating (seen in SEM images) that prevents the fiber/yarn movement.

Table 2. Weight and bending rigidity values of the fabrics

Sample	Weight (g/m^2) [S.D]	Bending rigidity (mg.cm) [S.D]
CV	64.96[a]	42.72
	[1.70]	[7.92]
CV-T	73.5[ab]	101.32
	[2.06]	[3.48]
CV-TF	79.34[b]	186.76
	[0.99]	[19.72]
CV-TFR$_1$	80.48[b]	189.12
	[3.97]	[19.73]
CV-TFR$_4$	98.14[c]	210.03
	[13.42]	[10.48]

Tensile stress-strain properties, the other mechanical performance, were evaluated and shown in Figure 14. According to Figure 14, the tensile strength of the samples increased with all coating types (from 66.45 N of reference to 92.8 N of TPU-SF@rGO$_4$) in machine direction (Figure 14 (a)) while decreased with composite coating including rGO particles in cross-machine direction. Enhancement in mechanical strength of the samples may a result of chemical interactions between the hydroxyl groups on the amino acid chains of SF and the amino groups (–NH) of TPU, as well as strong interfacial interactions with the fabric surface through increased hydrogen bonding within the TPU matrix, as can be seen in FT-IR spectra in Section 3.1. Also, the elongation values at break increased with composite coating in the both direction comparing the reference samples except TPU coated ones (Figure 14 (b)). Consequently, the resulting fabrics especially CV_TFR ones satisfy the requirements for practical wearing as well as heating performance.

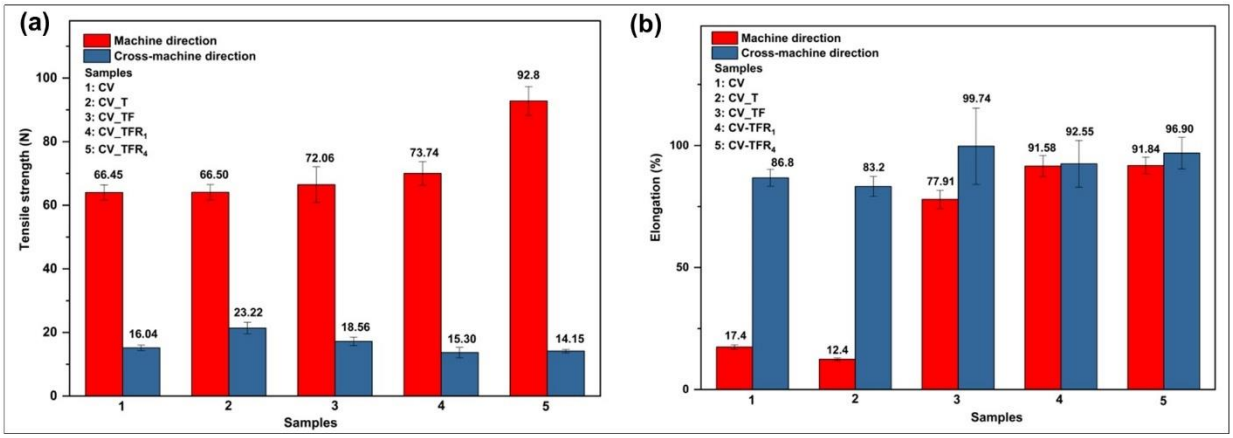


Figure 14. Mechanical properties of the fabrics, tensile strength (a) and elongation values (b) at break

Breathability, air and moisture permeability, is a crucial factor influencing wearability and comfortability of garment [47]. Air permeability, one of the permeability parameters, of the samples was evaluated to determine the effect of coating process and results were shown in Figure 15 (a). It is well known that air permeability giving an idea about heat and sweat transfer within in the fabric, varies depending on shape, volume, size, and number of the air flow channels hence porous structure. As seen in Figure 15 (a), although air permeability performance decreased with all coating types, significant

variability was only detected in samples containing SF and GO particles. This may be a result of very thin coating with TPU as seen in SEM images. Conversely, air permeability of the fabrics decreased from 2001.36 l/m²/s to 1614.5 and 1307 l/m²/s with TPU-SF and TPU-SF@rGO composite coating attributed to the thicker coating layer on fabric surface and also filling of some interspaces between fibers. Also, rGO particle content having crucial effect on heating performance, did not significant effect on the air permeability.

Adaptive moisture permeability performance especially has a decisive effect on end-use performance and also thermal comfort of the garments even in cold conditions with higher sweating due to physical activity. To further evaluate permeability hence comfortability of the samples, an adaptive moisture permeability test was executed at different RH values in the range of 40-65% at constant temperature of 20°C and results shown in Figure 15 (b). As seen in Figure 15 (b), TPU coating led to a significant decrease in WVP performance compared to reference and other composite coating treated ones, despite the thinner surface coating thickness detected in SEM images. Decreasing WVP with TPU coating is a result of hydrophobic character of polymer as confirmed by absorption capacity test, as well as pore blocking which prevents capillarity at both low and high relative RH values. On the other hand, CV_TF including SF particles (TPU-SF) possess the highest WVP performance at both low and high relative RH values. Besides, this sample exhibited a sensitive WVP to varying humidity, the higher relative humidity the higher WVP with the highest change rate of 16.18%. Also, the high WVP performance in this sample is followed by that of CV_TFR ones with varying rGO particle content. RH sensitive WVP performance in SF-included samples ascribed to hydrophilic nature of SF particles enabling bonding with water. Since SF is a protein substance containing tyrosine and serine with a high percentage of -OH groups in its structure, contact with sweat and/or water enables the -H bonds between the α-helix and β-sheet molecular structure to form reversible bonds with water molecules [39]. As a result, SF including samples (CV_TF and CV_TFR ones) exhibited a sensitive WVP to varying humidity, the higher relative humidity the higher WVP. On the other hand, hydrophobic character [48] of rGO particles cause a relative decrease in this RH-sensitive WVP performance, CV_TFR samples still have sensitive WVP performance comparing to reference and TPU-coated ones thanks to SF particles. These findings show that hydrophilicity and also ability of forming reversible bonds with water molecules may enable adaptive textile materials despite low porosity.

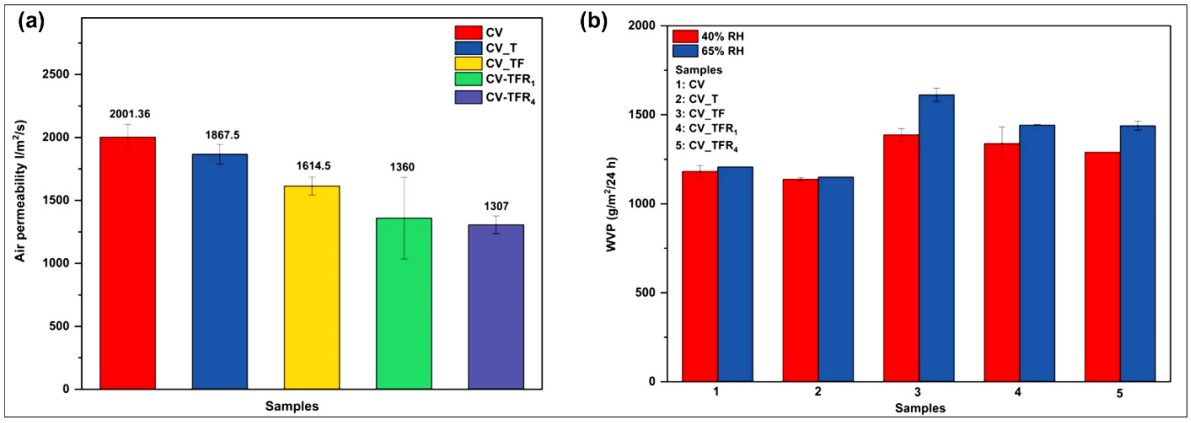


Figure 15. Air (a)and moisture permeability(b) of the fabrics

Besides permeability, moisture/water absorption capacity is a pivotal parameter influencing both thermal and moisture comfort under high-humidity conditions by promoting sweat evaporation and reducing the feeling of dampness [49], [50]. As shown in Figure 16, the water absorption capacity of the samples ranged between 533% and 845%. According to the results, while TPU coating led to significantly decrease in the absorption capacity rate due to hydrophobic character of TPU polymer compared to the CV, the opposite occurred for CV_TF ones. Maximum values belong to CV_TF samples with rate of 845% thanks to the hydrophilic nature of SF particles enabling bonding with water molecules in the composite

coating. Similar to WVP performance, adding hydrophobic [48] rGO particle with varying content resulted in lower absorption capacity rate comparing to refence samples but higher than CV_T ones.

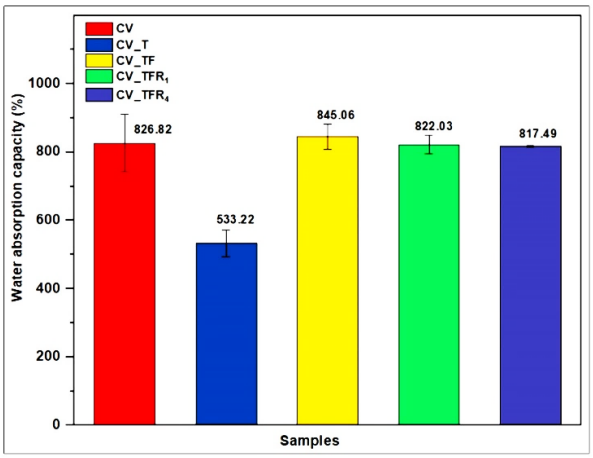


Figure 16. Water absorption capacity of the fabrics

Overall, these findings demonstrate that the adaptive permeability performance with enhanced mechanical and absorption properties of CV_TFR samples would greatly expand their application potential for practical applications.

4. CONCLUSIONS

In summary, a sustainable heating textile with adaptive permeability integrating passive indoor radiative heating, solar heating, and humidity hence sweat-sensitive moisture permeability was successfully developed for efficient personal thermal management in cold environments. The radiative-solar heating textile was fabricated via a simple spray-coating method, applying a composite coating of TPU matrix, SF particles regenerated from waste silkworm cocoons and rose-water reduced GO particles, onto CV-NFs. Owing to the enhanced solar absorptivity imparted by the rGO particles, CV_TFR samples especially including 4 wt.% of rGO particles have solar heating performance with 5.79°C and 1.96°C temperature increase under simulated conditions in dry and wet state, respectively. Also, the same sample has approximately 10.83°C, 8.13°C, and 10.93°C temperature increasing compared to the CV, cotton, and bare skin, respectively in real outdoor conditions. Besides its solar heating performance, the CV_TFR_4 sample exhibits passive indoor radiative heating, achieving a temperature increase of 2.01°C based on lower mid-infrared emissivity. Additionally, adaptive permeability performance with enhanced mechanical and absorption properties of CV_TFR samples make them practical for personal thermal management. This study opens up a promising direction for upcycling waste silkworm cocoons into high-value products with adaptive permeability and effective advanced heating textiles without any energy input.

Declaration of Ethical Standards

The authors declare compliance with all ethical guidelines, including authorship, citation, data reporting, and original research publication.

Credit Authorship Contribution Statement

Havvanur UYGUR: Investigation, formal analysis (all experiments, tests and analyses), validation, visualization, data curation.

Nazife KORKMAZ MEMİŞ: Conceptualization, methodology, investigation, supervision, resources, formal analysis (support), validation, visualization, data curation, writing - original draft, writing - review & editing.

Declaration of Competing Interest

The authors declare that they have no known competing financial interests or personal relationships that could have appeared to influence the work reported in this paper.

Funding / Acknowledgements

The authors would like to express appreciation for the support of the sponsors [Scientific and Technological Council of Türkiye (TUBITAK), 2209-A, Application No. 1919B012471315].

Data Availability

Data available on request from the authors.

Use of Artificial Intelligence

The authors confirm that no generative AI or AI-assisted technologies were used in in preparing, analysing, interpreting, or presenting the scientific data and conclusions in this manuscript.

5. REFERENCES

[1] C. Lan, F. Xu, C. Pan, Z. H. Guo, and X. Pu, "MXene based Janus fabrics with radiative heating towards efficient personal thermal management," *Chemical Engineering Journal,* vol. 472, p. 144662, 2023.

[2] S. Kaplan and N. Korkmaz Memiş, "Doğal radyasyonun yönetimiyle tasarlanan kişisel termal yönetim sağlayan pasif akıllı yapılar," *Tekstil ve Mühendis,* vol. 30, no. 131, pp. 210-225, 2023.

[3] X. Lan et al., "Designing heat transfer pathways for advanced thermoregulatory textiles," *Materials Today Physics,* vol. 17, p. 100342, 2021.

[4] B. Zhu et al., "Subambient daytime radiative cooling textile based on nanoprocessed silk," *Nature Nanotechnology,* vol. 16, no. 12, pp. 1342-1348, 2021.

[5] L. Lei et al., "Recent advances in thermoregulatory clothing: Materials, mechanisms, and perspectives," *ACS Nano*, vol. 17, no. 3, pp. 1803-1830, 2023.

[6] F. L. Zhu and Q. Q. Feng, "Recent advances in textile materials for personal radiative thermal management in indoor and outdoor environments," *International Journal of Thermal Sciences,* vol. 165, p. 106899, 2021.

[7] S. Xue, G. Huang, Q. Chen, X. Wang, and J. Fan, "Personal thermal management by radiative cooling and heating," *Nano-Micro Letters,* vol. 16, p. 153, 2024.

[8] Y. Wang et al., "Polydopamine adhesion of MXenes to cotton fabric for solar thermal and passive radiative heating," *Journal of Materials Science,* vol. 59, no. 8, pp. 3421–3435, 2024.

[9] J. Zhang et al., "An eco-friendly and multifunctional textile integrating radiative heating and cooling for large-temperature-variation personal thermal management," *Advanced Functional Materials,* p. 2419777, 2025.

[10] L. Cai et al., "Warming up human body by nanoporous metallized polyethylene textile," *Nature Communications*, vol. 8, no. 1, pp. 496, 2017.

[11] P. Hsu et al., "A dual-mode textile for human body radiative heating and cooling," *Science Advances,* vol. 3, p. e1700895, 2017.

[12] H. Luo et al., "An ultra-thin colored textile with simultaneous solar and passive heating abilities," *Nano Energy,* vol. 65, p. 103998, 2019.

[13] Q. Li, J. Lu, P. Gupta, and M. Qiu, "Engineering optical absorption in graphene and other 2D materials: advances and applications," *Advance Optical Materials,* vol. 7, no. 20, p. 1900595, 2019.

[14] M. Furchi et al., "Microcavity-integrated graphene photodetector," *Nano Letters,* vol. 12, no. 6, pp. 2773-2777, 2012.

[15] L. Zhu et al., "Angle-selective perfect absorption with two-dimensional materials," *Light: Science & Applications,* vol. 5, no. 3, pp. e16052-e16052, 2016.

[16] S. Thongrattanasiri, F. H. Koppens, and F. J. G. De Abajo, "Complete optical absorption in periodically patterned graphene," *Physical Review Letters,* vol. 108, no. 4, p. 04740, 2012.

[17] Z. Fang et al., "Gated tunability and hybridization of localized plasmons in nanostructured graphene," *ACS Nano,* vol. 7, no. 3, pp. 2388-2395, 2013.
[18] T. L. Liu, K. J. Russell, S. Cui, and E. L. Hu, "Two-dimensional hybrid photonic/plasmonic crystal cavities," *Optic Express,* vol. 22, no. 7, pp. 8219-8225, 2014.
[19] J. R. Piper and S. Fan, "Total absorption in a graphene monolayer in the optical regime by critical coupling with a photonic crystal guided resonance," *ACS Photonics,* vol. 1, no. 4, pp. 347-353, 2014.
[20] M. Grande et al., "Graphene-based perfect optical absorbers harnessing guided mode resonances," *Optic Express,* vol. 23, no. 16, pp. 21032-21042, 2015.
[21] L. Huang et al., "Atomically thin MoS_2 narrowband and broadband light superabsorbers," *ACS Nano,* vol. 10, no. 8, pp. 7493-7499, 2016.
[22] X. Yue et al., "Laminated fibrous membrane inspired by polar bear pelt for outdoor personal radiation management," *ACS Applied Materials & Interfaces,* vol. 12, no. 10, pp. 12285-12293, 2020.
[23] Y. Wang et al., "Multifunctional polyimide aerogel textile inspired by polar bear hair for thermoregulation in extreme environments," *Chemical Engineering Journal,* vol. 390, p. 124623, 2020.
[24] Y. E. Woo and K. W. Oh, "Fabrication of polyester fabrics with tungsten bronze nanorods and a silane coupling agent for improved thermal storage and washing durability," *Fashion and Textiles,* vol. 10, no. 1, pp. 1-12, 2023.
[25] T. F. Chala et al., "Highly efficient near infrared photothermal conversion properties of reduced tungsten oxide/polyurethane nanocomposites," *Nanomaterials,* vol. 7, no. 7, p. 191, 2017.
[26] X. Liu et al., "Multifunctional AgNW@MXene decorated polymeric textile for highly-efficient electro-/photothermal conversion and triboelectric nanogenerator," *Composites Part A: Applied Science and Manufacturing,* vol. 156, p. 106883, 2022.
[27] J. Dong et al., "MXene-coated wrinkled fabrics for stretchable and multifunctional electromagnetic interference shielding and electro/photo-thermal conversion applications," *ACS Applied Materials & Interfaces,* vol. 13, no. 50, pp. 60478-60488, 2021.
[28] H. Pu et al., "Polydopamine modified CuS particles filled cellulose fiber for photothermal conversion performance," *Industrial Crops and Products,* vol. 193, p. 116188, 2023.
[29] Y. V. Lee and B. Tian, "Learning from solar energy conversion: biointerfaces for artificial photosynthesis and biological modulation," *Nano Letters,* vol. 19, no. 4, pp. 2189-2197, 2019.
[30] G. Lan et al., "Sustainable carbon materials toward emerging applications," *Small Methods*, vol. 5, no. 5, p. 2001250, 2021.
[31] W. Luo et al., "Efficient enhancement of photothermal conversion of polymer-coated phase change materials based on reduced graphene oxide and polyethylene glycol," *Journal of Energy Storage*, vol. 78, p. 109950, 2024.
[32] L. Lei et al., "Toward low-emissivity passive heating: a supramolecular-enhanced membrane with warmth retention," *Materials Horizons,* vol. 10, no. 10, pp. 4407-4414, 2023.
[33] B. Haghighi and M. A. Tabrizi, "Green-synthesis of reduced graphene oxide nanosheets using rose water and a survey on their characteristics and applications," *RSC Advances,* vol. 3, no. 32, pp. 13365-13371, 2013.
[34] B. N. Kumila, N. Zaidah, and H. H. Kusuma, "Green reduction of graphene oxide (GO) from coconut shell using rose water in various temperature," *Jurnal Fisika dan Aplikasinya,* vol. 18, no. 2, pp. 48-52, 2022.
[35] A. Ahmed, A. Singh, S. J. Young, V. Gupta, M. Singh, and S. Arya, "Synthesis techniques and advances in sensing applications of reduced graphene oxide (rGO) composites: A review," *Composites Part A: Applied Science and Manufacturing,* vol. 165, p. 107373, 2023.
[36] X. Zhao, L. Y. Wang, C. Y. Tang, X. J. Zha, Y. Liu, B. H. Su, et al., "Smart $Ti_3C_2T_x$ MXene fabric with fast humidity response and joule heating for healthcare and medical therapy applications," *ACS Nano,* vol. 14, no. 7, pp. 8793-8805, 2020.

[37] C. Lan et al., "Humidity-responsive actuator-based smart personal thermal management fabrics achieved by solar thermal heating and sweat-evaporation cooling," *ACS Nano,* vol. 19, no. 8, pp. 8294-8302, 2025.
[38] T. Xue et al., "Integration of dynamic thermochromism and reversible moisture transport in hierarchically designed fabric for adaptive personal thermal management," *Chemical Engineering Journal*, vol. 507, p. 160826, 2025.
[39] M. Oliver-Cadena, G. Santos-Lopez, E. O. Figueroa-Pérez, F. M. L. Martínez, M. A. Karaaslan, S. Renneckar, and M. C. Gutiérrez, "Thermo-activated shape memory films based on chitosan reinforced with silk fibroin, obtained by an environmentally friendly process using a deep eutectic solvent," *Journal of Polymers and the Environment,* vol. 33, no. 2, pp. 760-776, 2025.
[40] X. Shan, L. Liu, Y. Wu, D. Yuan, J. Wang, C. Zhang, and J. Wang, "Aerogel-functionalized thermoplastic polyurethane as waterproof, breathable freestanding films and coatings for passive daytime radiative cooling," *Advanced Science,* vol. 9, no. 20, p. 2201190, 2022.
[41] J. Xia et al., "High thermal conductivity and radiative cooling designed boron nitride nanosheets/silk fibroin films for personal thermal management," *ACS Applied Materials & Interfaces,* vol. 16, no. 6, pp. 7732-7741, 2024.
[42] Z. Wen et al., "Tough and transparent supramolecular cross-linked co-assembled silk fibroin films for passive radiative cooling," *Advanced Functional Materials,* vol. 34, no. 42, p. 2406920, 2024.
[43] L. Tang et al., "Waste cotton fabric-derived multimodal heating textile for comfortable and reliable personal thermal management," *Journal of Cleaner Production,* vol. 425, p. 138992, 2023.
[44] N. Murugesan et al., "Enhancing selectivity of solar absorber using reduced graphene oxide modified nickel oxide nanocomposite thin films," *Solar Energy,* vol. 247, pp. 185-195, 2022.
[45] T. Wu et al., "Tai Chi-inspired solar/electro-driven multimode cellulose fabric heater for all-day wearable thermal comfort," *ACS Applied Polymer Materials,* vol. 7, no. 10, pp. 5820-5833, 2025.
[46] Z. Li et al., "Durable asymmetric silk fabric with rapid heat conduction, spectral selectivity and sweat transfer capabilities for effective personal thermal-moisture management," *Journal of Colloid and Interface Science,* vol. 689, p. 137203, 2025.
[47] H. Guo et al., "Photonic metafabric with biomimetic triangular light track for passive radiative cooling," *Advanced Fiber Materials,* vol. 7, no. 1, pp. 106-116, 2025.
[48] Z. Tang et al., "One-step synthesis of hydrophobic-reduced graphene oxide and its oil/water separation performance," *Journal of Materials Science,* vol. 51, no. 19, pp. 8791-8798, 2016.
[49] K. H. Chau et al., "Infrared identification of wetted fabric by monitoring dry-to-wet transition," *Measurement,* p. 118060, 2025.
[50] Z. Zeng et al., "Janus hygroscopic-cooling fabric (J-HCF) based on filament/bamboo core yarns for personal thermal-moisture management," *Cellulose,* vol. 32, no. 2, pp. 1339-1354, 2025.